Sonochemical Synthesis of SnO_2 Nanoparticles and Their Preliminary Study as Li Insertion Electrodes

Junjie Zhu,† Zhonghua Lu, S. T. Aruna, Doron Aurbach,* and Aharon Gedanken*

Department of Chemistry, Bar-Ilan University, Ramat-Gan 52900, Israel

Received October 26, 1999

SnO_2 semiconductor nanoparticles were synthesized by an ultrasonic irradiation of an aqueous solution of $SnCl_4$ and azodicarbonamide under ambient air. These nanoparticles are ∼3−5 nm in size, as calculated using the Debye−Scherrer formula, and as observed by TEM. The SnO_2 nanoparticles were also characterized by powder X-ray diffraction (XRD), reflection spectroscopy and FT-IR spectroscopy, transmission electron microscopy (TEM), DSC, and TGA. The band gap was calculated from reflection spectroscopy. Electrochemical tests were performed using the SnO_2 nanoparticles as the electrode's materials in nonaqueous Li salt solutions. The results showed promising reversibility, cycle life and high capacity for lithium insertion into the SnO_2 nanoparticles.

1. Introduction

Semiconductor nanoparticles have been extensively studied from both experimental and theoretical viewpoints, owing to their potential applications in solar energy conversion, photocatalysis, and optoelectronic industry.[1−4] SnO_2 is an n-type semiconductor with a large band gap, and is well-known for its applications in gas sensors[5,6] and dye-based solar cells.[7] In recent years, attention has been focused on its possible application in electrochromic devices.[8] Lithium ions can be electrochemically inserted into a transparent SnO_2 electrode, resulting in the change of the optical transmittance.[9] In recent years there has been an increasing interest in the use of SnO_2 as an anode material for lithium batteries, starting with the announcement by Fuji Photo Film Celltee Co. Ltd., Japan, about their STALION lithium ion cell.[10] These cells utilized an amorphous tin-based composite oxide as the anode (together with a Li_xCoO_2 cathode). It appeared that the basic anode process in these cells is lithium insertion into tin oxides, which form Li−Sn alloys in a matrix of Li_2O.[11] Hence, the reversible process that finally remains is lithium alloying with metallic tin. In fact, Li−Sn alloys were already suggested many years ago as a substitute for Li metal anodes in rechargeable Li batteries. Li can reversibly alloy with tin up to a stoichiometry of $Li_{22}Sn_5$. Lithiation of tin forms different phases, including Li_2Sn_5 (∼0.6 V, Li/Li^+), LiSn (∼0.45 V, Li/Li^+), and Li_7Sn_3, Li_5Sn_2, $Li_{13}Sn_5$, Li_7Sn_2, $Li_{22}Sn_5$ at a potential range between 0.4 and 0 V vs Li/Li^+).[12−14]

The electrochemical behavior of Li electrodes in any polar aprotic electrolyte solution depends on their passivation. Lithium metal reacts with most of the relevant polar aprotic solvents, salt anions (except halides), and atmospheric contaminants. The reaction products (which are organic and inorganic Li salts), usually precipitate as thin Li ion conducting films on the active metal surface. In rechargeable batteries, repeated Li deposition−dissolution leads to pronounced morphological changes which adversely affect the stability of these surface films, which in fact protect the active metal from continuous reactions with solution species. Instability of the passivating films on lithium leads to continuous reactions of the active metal with solution components during prolonged charge−discharge cycling. In addition, the surface films formed on lithium in a large variety of electrolyte solutions are nonuniform, and thus induce nonuniform current distribution that leads to dendrite formation (which can short the battery systems). Thereby, the reversibility

* Corresponding authors. E-mail: gedanken@mail.biu.ac.il. E-mail: aurbach@mail.biu.ac.il. Fax: +972-3-5351250.

† Permanent address: Department of Chemistry, Nanjing University, Nanjing, 210093, China.

(1) Peng, X.; Schlamp, M. C.; Kadavanich, A. V.; Alivisatos, A. P. *J. Am. Chem. Soc.* **1997**, *119*, 7019.

(2) Golan, Y.; Margulis, L.; Hodes, G.; Rubinstein, I.; Hutchinson, J. L. *Surf. Sci.* **1994**, *311*, L633.

(3) Henglein, A.; Bunsen-Ges, Ber. *J. Phys. Chem.* **1995**, *99*, 903.

(4) Kamat, P. V.; Shanghavi, B. *J. Phys. Chem. B* **1997**, *101*, 7675.

(5) Ansari, G.; Boroojerdian, P.; Sainkar, S. R.; Karekar, R. N.; Aiyer, R. C.; Kulkarni, S. K. *Thin Solid Films* **1997**, *295*, 271.

(6) Varghese, O. K.; Malhotra, L. K. *Sens. Actuators B* **1998**, *53*, 19.

(7) Ferrere, S.; Zaban, A.; Gsegg, B. A. *J. Phys. Chem B* **1997**, *101*, 4490.

(8) Olivi, P.; Pereira, E. C.; Longo, E.; Varella, J. A.; Bulhoes, L. O. d. S. *J. Electrochem. Soc.* **1993**, *140*, L81.

(9) Mckinnon, W. R.; Haering, R. R. *Modern Aspects of Electrochemical*; White, R. E., Bockis, J. O'M., Conway, B. E., Eds.; Plenum: New, York, 1983; No. 15.

(10) *Nippon Denki Shibun*, March 11, 1996.

(11) Fuji Photo Film Co., Ltd., Euro. Pat. 0,651,450, A1, 1995.

(12) N. Winter, N.; Besenhard, J. O. Electrochemical lithiation of tin based intermetallic compounds and composites. *Electrochim. Acta* **1999**, *45*, 31.

(13) Liu, W. F.; Huang, X. J.; Wang, Z. X.; Li, H.; Chen, L. Q. *J. Electrochem. Soc.* **1998**, *145*, 59.

(14) Brousse, T.; Retoux, R.; Herterich, U.; Schleich, D. M. *J. Electrochem. Soc.* **1998**, *145*, 1.

10.1021/cm990683l CCC: $19.00
Published on Web 08/09/2000

and the cycle life of Li metal anodes in rechargeable batteries are so limited.[15]

It was believed that the replacement of the Li metal anode in rechargeable batteries by an Li−Sn alloy may considerably lower the volume changes during charge−discharge of the Li anode, which leads to its instability and limited reversibility, due to repeated irreversible reactions with solution species.[10−14] However, as nicely summarized and demonstrated in ref 12, insertion of lithium into tin particles also leads to morphological changes. The potentials of Li−Sn alloying (<0.5 V vs Li/Li^+) are sufficiently low for these alloys to be considered as very active surface for **all** commonly used electrolyte solutions comprised of Li salts in polar aprotic solvents. Hence, the stability of Li−Sn alloys in these electrolyte solutions also depends on surface film formation and passivation. It is thereby expected that the reversibility of Li−Sn alloys in electrochemical Li insertion processes depends strongly on the possibility of stabilizing these surface films during prolonged charge−discharge cycling, and hence, the morphology of the particles which interact with the solution may play a critical role in determining the performance of Li−Sn alloys as practical anodes in rechargeable Li batteries.[10−14] From recent papers, it can be concluded that using SnO_2 as the starting material, instead of tin in Li insertion processes, leads to pronounced stabilization of the Li−Sn alloys thus formed due to the formation of Li_2O. Hence, the active mass becomes a matrix of Li oxide in which Li−Sn particles are embedded, thus providing enhanced stability to these systems during repeated charge−discharge (lithiation−delithiation) processes, probably because this matrix can be batter passivated by the surface films formed in solution than agglomerates of Li−Sn particles with no addition interphase.[16]

A variety of methods, such as sol−gel,[17,18] chemical vapor deposition,[19] magnetron sputtering,[20] evaporation of elemental tin in an oxygen atmosphere[21] have been used to prepare SnO_2 particles and films.

Hence, the importance of Li−tin alloys and tin oxides in relation to high-energy density, rechargeable batteries, as described above, justifies intensive material research on these compounds, and an extensive search for useful methods for their preparation.

Currently, the sonochemical method has been used extensively to generate novel materials with unusual properties (e.g., formation of nanophased amorphous materials).[22] The chemical effects of ultrasound arise from acoustic cavitation, that is, the formation, growth, and implosive collapse of bubbles in a liquid. The implosive collapse of the bubbles generates a localized hotspot through adiabatic compression or shock wave formation within the gas phase of the collapsing bubble. The conditions formed in these hotspots have been experimentally determined, with transient temperatures of ~5000 K, pressures of 1800 atm,[23] and cooling rates in excess of 10^{10} K/s. These extreme conditions attained during bubble collapse have been exploited to decompose the metal−carbonyl bonds and generate metals,[23−26] metal carbides,[27] and metal oxides and sulfides.[28] This method is a simple and effective route for preparing fine powders on a nanometer scale and with homogeneous particle size distribution.

In the present work, we report on a sonochemical method for the preparation of SnO_2 semiconductor nanoparticles. SnO_2 nanoparticles were prepared by the ultrasonic irradiation of an aqueous solution of $SnCl_4$ and azodicarbonamide in air. The as-prepared nanoparticles are approximately 3−5 nm in size, as calculated using the Debye−Scherrer formula[29] and as seen by TEM. The band gap was calculated from reflection spectroscopy and found as 4.05 eV. The characterization also included a study of these SnO_2 nanoparticles as received and after heat treatment, as an active mass in reversible lithium insertion electrodes. The electrochemical measurements indeed showed some promising features of these materials.

2. Experimental Section

a. Materials. $SnCl_4$ (99.9%) and azodicarbonamide (Aldrich), 1-methyl-2-pyrrolidone (Fluka), doubly distilled water, and absolute ethanol (Pharmco Inc.) were used. Highly pure, ready to use Li salt solutions ($LiPF_6$/EC-DEC, etc.) for the electrochemical measurements were obtained from Merck KGaA.

b. Instrumentation. The instruments used in this work for TEM, XRD, FT-IR, DSC, TGA, and reflection measurements have been described elsewhere.[28] An Arbin Inc. computerized, multichannel battery tester (Model 2000) was used for the electrochemical study of SnO_2 electrodes. The charge−discharge behavior of the cells containing composite SnO_2 electrodes and lithium foil counter electrodes was measured galvanostatically ($0.2mA/cm^2$) in the 10m V to 1.3 V range vs Li/Li^+.

c. Preparation of SnO_2 Nanoparticles. About 2 g of $SnCl_4$ and 0.3 g of azodicarbonamide were dissolved in 70 mL of doubly distilled water and were sonicated for 2 h in air at room temperature. A round-bottomed Pyrex glass vessel (total volume- 70 mL) was used for the ultrasound irradiation. The temperature of the mixture rose gradually to 80 °C during ultrasonic irradiation. After sonication for 2 h, the solution was centrifuged and washed with water, and then washed several times with absolute ethanol. The density of the various SnO_2 samples was also calculated, both as a powder and in compressed pellets. Knowing the density of the compressed SnO_2 samples is important for calculating the voltammetric

(15) Aurbach, D.; Zaban, A.; Ein-Eli, Y.; Weissman, I.; Markovsky, B.; et al. *J. Power Sources* **1995**, *54*, 76; **1997**, *86*, *91*.
(16) Courtney, I. A.; Dahn, J. R. *J. Electrochem. Soc.***1997**, *144*, 2045, 2943.
(17) Wang, D.; Wen, S.; Chen, J.; Zhang, S.; Li, F. *Phys. Rev. B* **1994**, *49*, 14282.
(18) Maddalena, A.; Del Maschio, R.; Dire, S.; Raccanelli, A. *J. Non-Cryst. Solids* **1990**, *121*, 365.
(19) Tarey, R. D.; Raju, T. A. *Thin Solid Films* **1995**, *128*, 181.
(20) Minami, T.; Nanto, H.; Takata, S. *Jpn. J. Appl. Phys.* **1988**, *27*, L287.
(21) Schlosser, V.; Wind, G. In Proceedings of the 8th EC photovolltaic Solar Energy Conference, p 998, Florence, Italy, 1998.
(22) *Ultrasound: Its Chemical, Physical and Biological Effects*; Suslick, K. S. Ed.; VCH: Weinheim, 1988.
(23) Suslick, K. S.; Choe, S. B.; Cichowlas, A. A.; Grinstaff, M. W. *Nature* **1991**, *353*, 414.
(24) Koltypin, Yu.; Katabi, G.; Prozorov, R.; Gedanken, A. *J. Non-Cryst. Solids* **1996**, *201*, 159.
(25) Nagata, Y.; Mizukoshi, Y.; Okitsu. K.; Maeda, Y. *Radiation Res.* **1996**, *146*, 333.
(26) Okitsu, K.; Mizukoshi, Y.; Bandow, H.; Maeda, Y.; Yamamoto, T.; Nagata, Y. *Ultrason. Sonochem.* **1996**, *3*, 249.
(27) Hyeon, T.; Fang, M.; Suslick, K. S. *J. Am. Chem. Soc.* **1996**, *118*, 5492.
(28) Cao, X.; Koltypin, Yu.; Katabi, G.; Felner, I.; Gedanken, A. *J. Mater. Res.* **1997**, *12*, 405L. Arul Dhas, N.; Gedanken, A. *J. Phys. Chem. B* **1997**, *11*, 9495. Arul Dhas, N.; Zaban, A.; Gedanken, A. *Chem. Mater.* **1999**, *11*, 806.
(29) *X-ray Diffraction Procedure*; Klug, H., Alexander, L., Eds.; Wiley: New York, 1962; p125.

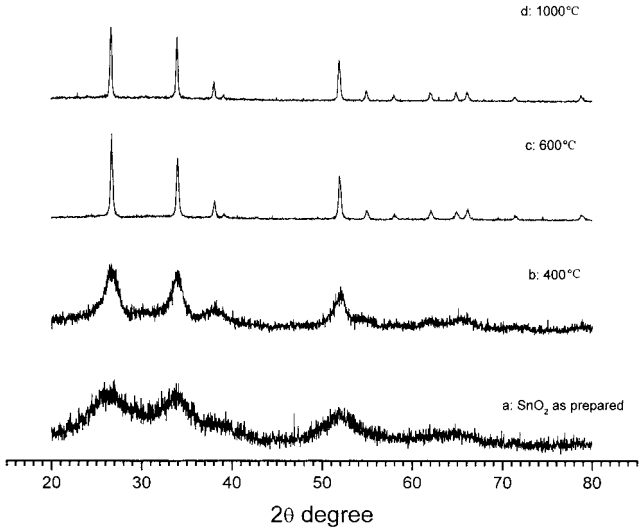

Figure 1. X-ray diffraction patterns of as-prepared and heat-treated SnO_2 nanoparticles: (a) as-prepared SnO_2; (b) sintered at 400 °C; (c) 600°; and (d) 1000 °C.

capacity (mAh/L) of the various SnO_2 samples that were tested as Li insertion electrodes. The density of powdered as received SnO_2, and samples heated to 400 °C and 1000 °C was 1.0, 1.7, and 1.8 g/cm^3, respectively. The density of the compressed samples was between 3.4 and 3.5 g/cm^3.

d. Electrochemical Behavior of SnO_2 Electrodes. The working electrodes of the as-prepared or heat-treated SnO_2 were fabricated by coating slurries of the respective SnO_2 powder (55 wt %), carbon black (30 wt %), and polyvinylidene fluoride (PVDF, 15 wt %) dissolved in 1-methyl-2-pyrrolidone, on copper foil substrates. The thickness of the coated film was about 80 μm. After coating, the electrodes were dried at 120 °C for 24 h and pressed between two plates at 40 atm. The electrodes were cut into 1.0 cm^2 squares and weighed. Standard coin-type test cells were constructed using these working electrodes and Li counter electrodes separated by a polypropylene microporous separator. The electrolyte used was a 1 M solution of $LiPF_6$ dissolved in a 50:50 mixture by volume of ethylene carbonate (EC) and diethyl carbonate (DEC). A 1.0 cm^2 lithium foil was used as the counter electrode. Cells were assembled crimped under highly pure argon atmosphere in a VAC Inc. glovebox (water and oxygen concentrations were usually less than 5 ppm). All the cells were tested with a constant current and were charged and discharged between fixed predetermined voltage limits. In independent measurements we found that the carbon black used as an additive does not insert lithium at a significant capacity. Hence, the capacity measured in the Li insertion processes of the electrodes should only be attributed to the active mass (SnO_2).

3. Results and Discussion

XRD studies. Figure 1 shows the XRD patterns of as-prepared and heat-treated SnO_2 under different temperatures. The XRD pattern of the as-prepared SnO_2 showed the presence of very broad peaks (Figure 1a). The broad peaks indicate either particles of very small crystalline size or particles which are semicrystalline in nature.[29] The peak positions fit well with previously reported values of a SnO_2 phase (JCPDS 41-1445). The size of the as-prepared SnO_2 nanoparticles estimated from the Debye−Scherrer formula is about 3 nm. As-prepared SnO_2 nanoparticles were sintered at 200, 400, 600, 800, and 1000 °C for 5 h. It was found that their XRD peaks become gradually sharper with increasing temperature, indicating the increase in crystal size due to the sintering process that the particles undergo.

TEM Studies. The TEM observations for the as-prepared and heat-treated SnO_2 nanoparticles are shown in Figure 2. It is apparent that as-prepared SnO_2 nanoparticles are spherical, and the particles are held together by a porous irregular network. The average size of these nanoparticles is in the range of 1−5 nm, which is in good agreement with the XRD result. After the SnO_2 is heated at different temperatures, the particle size of the SnO_2 increases gradually. A large increase in particle size is observed after sintering at 800 °C, with the particles having the appearance of rounded hexagons (Figure 2 e,f), exhibiting a high degree of crystallinity. The particle size distribution, measured directly from TEM micrographs are shown as histograms in Figure 3. Average particle sizes of 3, 6, 9, 20, 44, and 62 nm were obtained for the as-prepared SnO_2 and the sintered material at 400, 600, 800, and 1000 °C, respectively.

DSC and TGA Studies. The DSC curves presented in Figure 4 reveal a distinct exothermic peak at 200 °C, which may be attributed to an irreversible amorphous → crystalline transition. This conclusion is supported by the fact that this peak did not appear when this measurement was repeated and the same sample was reheated over the same temperature range. The structural analysis of the as-prepared SnO_2 cannot rule out the possibility that the sonochemical synthesis in fact produces a mixture of amorphous and nanocrystalline SnO_2 particles. Figure 5 shows the rate of weight loss of the particles as a function of temperature, as measured by thermogravimetric analysis. The particles show a weight loss (15.30%) between 50 and 450 °C. The higher rate of weight loss (8.73%) was observed between 50 and 120 °C, which can come from the evaporation of physically adsorbed water and NH_3 on the surface and in pores of the particles. In the DSC curve, an endothermic peak appears at the same temperature. Another weight loss (4.94%) from 150 to 250 °C may come from the decomposition of $Sn(OH)_4$. A further small weight loss (1.88%) takes place steadily between 260 and 450 °C, and which may be attributed to the continuous removal of chemically adsorbed water, which may be related to different types of surface hydroxyl group condensation.[30] Above 450 °C, no weight loss is observed in the TGA curve.

FT-IR Spectroscopy Studies. As-prepared SnO_2 exhibits an intense, very broad IR peak ranging from ∼3600 to ∼2500 cm^{-1}, with two maxima at ∼3430 and ∼3150 cm^{-1}, which may be due to adsorbed water and NH_3. The N−H band observed around ∼3150 cm^{-1} may be due to the use of azodicarbonamide to promote the $SnCl_4$ hydrolysis, which leads to the formation of ammonia. After calcination, the peak at 3430 cm^{-1} shift to higher wavenumbers, while the peak at 3150 cm^{-1} disappears. The bands centered at ∼1630 cm^{-1} and ∼1415 cm^{-1} may also be related to water and NH_3. The peaks around 2350 cm^{-1} belong to residual CO_2 traces in the spectrometer's atmosphere, while the peaks at the low wavenumber (<800 cm^{-1}) should be attributed

(30) Harrison, P. G.; Guest, A. J. *J. Chem. Soc, Faraday Trans.* **1987**, *83*, 3383.

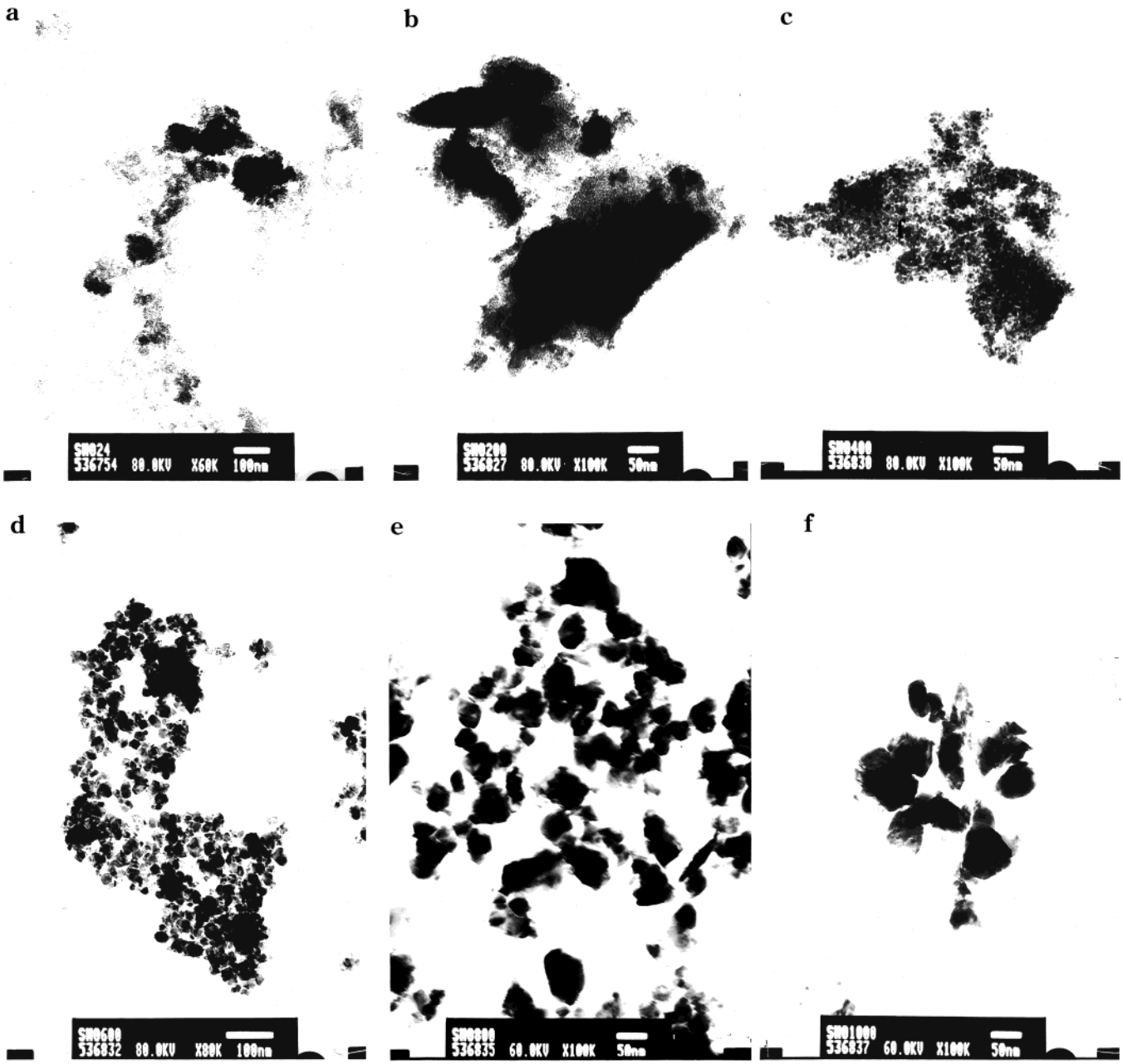

Figure 2. Transmission electron micrographs of the SnO_2 nanoparticles: (a) as-prepared; (b) sintered at 200 °C; (c) 400 °C; (d) 600 °C; (e) 800 °C; and (f) 1000 °C.

to the SnO_2. Increasing the calcination temperature results in the decrease of the intensity of the water band (see, for example, the comparison between the spectra related to 25 and 200 °C in Figure 6), and after heating at 400 °C, the bands attributed to NH_3 around 3150 and 1415 cm^{-1} disappear. After calcination at 1000 °C, the band corresponding to water at ∼3430 cm^{-1} almost disappears. However, we could still observe a very small weak peak ∼3480 cm^{-1}, which is probably due to the fact that the spectra were not recorded in situ and some readsorption of water from the ambient atmosphere has occurred. The bands observed in the range 850−1350 cm^{-1} in the IR spectra may be assigned to a hydroxyl bending mode of different types of surface hydroxyl groups. The IR bands at 970 and 1260 cm^{-1} are reduced in intensity with increasing temperature. Only traces of these two bands remain after heating at 400 °C and are completely absent at 600 °C. Two intense broad bands at ∼674 and ∼550 cm^{-1} for as-prepared SnO_2 are also observed. After calcination at 400 °C, the intensity of these peaks decreases and a new peak appear at 614 cm^{-1}. With the increase in temperature, the intensity of the peak at 614 cm^{-1} increases. After sintering at 1000 °C, the peak at 674 cm^{-1} almost disappears, while the peak at 614 cm^{-1} almost reaches a maximum. This band is assigned to the antisymmetric Sn−O−Sn stretching mode of the surface-bridging oxide formed by condensation of adjacent surface hydroxyl groups (which produce water). Similarly, the peak at 550 cm^{-1} also disappears gradually and a new peak appears at ∼470 cm^{-1}, which is assigned to a symmetric Sn−O−Sn stretching mode.[30,31] These spectral changes can be easily attributed to changes in the size and the shape

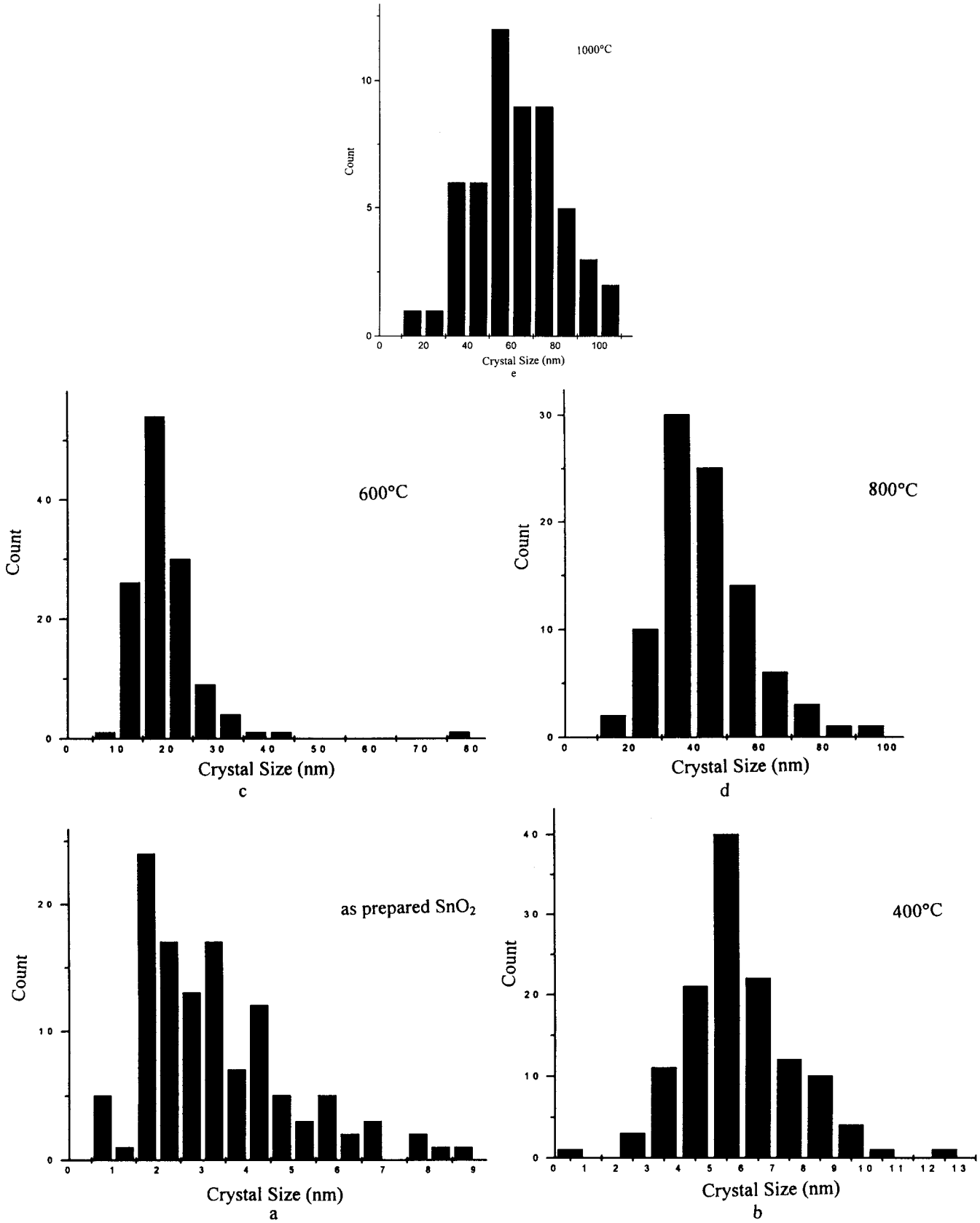

Figure 3. The particle size distribution picture measured directly from TEM: (a) as-prepared SnO_2; (b) sintered at 400 °C; (c) 600 °C; (d) 800 °C; and (e) 1000°.

of the SnO_2 particles, since it is known that for SnO_2 particles of different size and shape, the anti symmetric and symmetric Sn−O−Sn IR bands can appear at a different wavenumber.[32]

(31) Harrison, P. G.; Lloyd, N. C.; Daniell, W.; Bailey, C.; Azelee, W. *Chem. Mater.* **1999**, *11*, 896.

(32) Ocana, M.; Serna, C. J.; Matijevic, E. *Colloid Polym. Sci.* **1995**, *273*, 681.

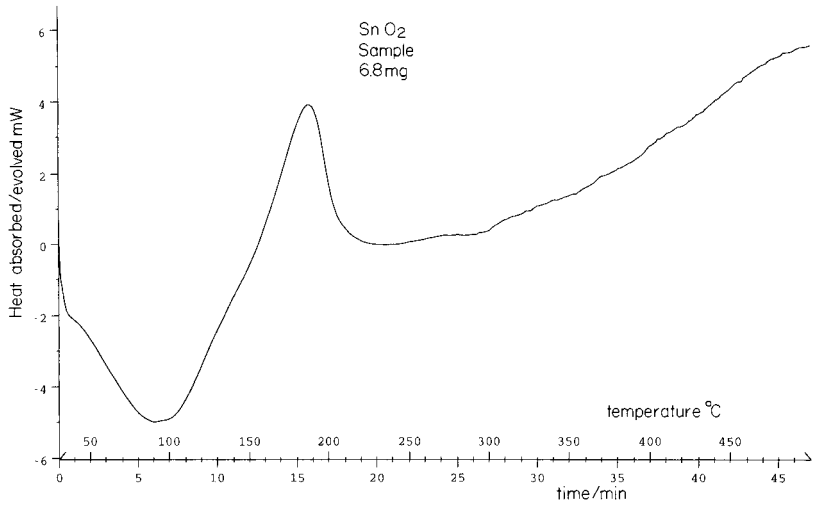

Figure 4. DSC curve of as-prepared SnO_2.

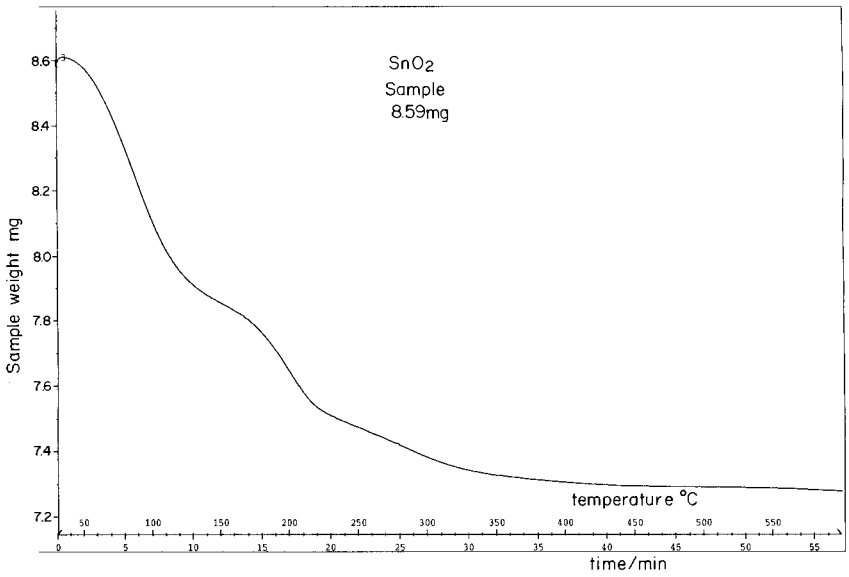

Figure 5. TGA curve of as-prepared SnO_2.

Reflectance. We have carried out reflection spectra measurements of SnO_2 powder to resolve the excitonic or interband (valence-conduction band) transitions of SnO_2, which allow us to calculate the band gap. The SnO_2 sample was spin coated using ethanol on glass to form a film. The energy band gap of these films was calculated with the help of reflection spectra. To measure the energy band gap, we used the Tauc relation in which a graph between $(\alpha h\nu)^2$ vs $h\nu$ is plotted, where α is the absorption coefficient and $h\nu$ is the photon energy. The absorption coefficient α is proportional to $\log [(R_{max} - R_{min})/(R - R_{min})]$ where reflectance falls from R_{max} to R_{min} due to the absorption by the material (R is the reflectance for any intermediate photons[33]). Hence, we have used α in terms of reflectance as $\log [(R_{max} - R_{min})/(R - R_{min})]$ and computed the energy band for the material. Figure 7 presents the optical reflection spectra of the SnO_2 powder, and Figure 8 is a plot of $\{\log[(R_{max} - R_{min})/(R - R_{min})]\}^2$ vs $h\nu$. The band gap calculated from the curve of an as-prepared sample is 4.05 eV. The value of the band gap energy is larger than that of the reported value for bulk SnO_2 (3.7 eV),[34,35] which was also attributed to SnO_2 nanoparticles. Similarly, we have also calculated the band gap of SnO_2 heat-treated at 600 °C, to be 3.78 eV, This value is smaller than that of as-prepared SnO_2, but close to that of bulk SnO_2. As already reported,[36] very small particles have a large band gap due to quantum size effects. This explains the fact that the sonochemically prepared SnO_2 (of nanometer size) has a larger band gap than the commercially available bulk SnO_2.

Electrochemical Behavior. The potential of the sonochemically synthesized SnO_2 particles of the nanometer size as the active mass in reversible lithium insertion electrodes was examined in preliminary galvanostatic tests of composite electrodes containing SnO_2, carbon, and binder, as described in the Experimental Section. The solution chosen for these tests was EC-DMC/$LiPF_6$, which is a commonly used electrolyte solution for Li ion batteries. Figure 9 shows chronopotentiograms obtained during a first lithiation−

(33) Sharma, S. K.; Kumar, V.; Kaushish, S. K.; Sharma, T. P.; Sharma, S. K. *Solid State Phenom.* **1997**, *55*, 40.

(34) Memming, R. *Electrochim. Acta* **1980**, *25*, 77.
(35) Vogel, R.; Hoyer, P.; Weller, H. *J. Phys. Chem.* **1994**, *98*, 3183.
(36) Gorer, S.; Hodes, G. *J. Phys. Chem.* **1994**, *98*, 5338.

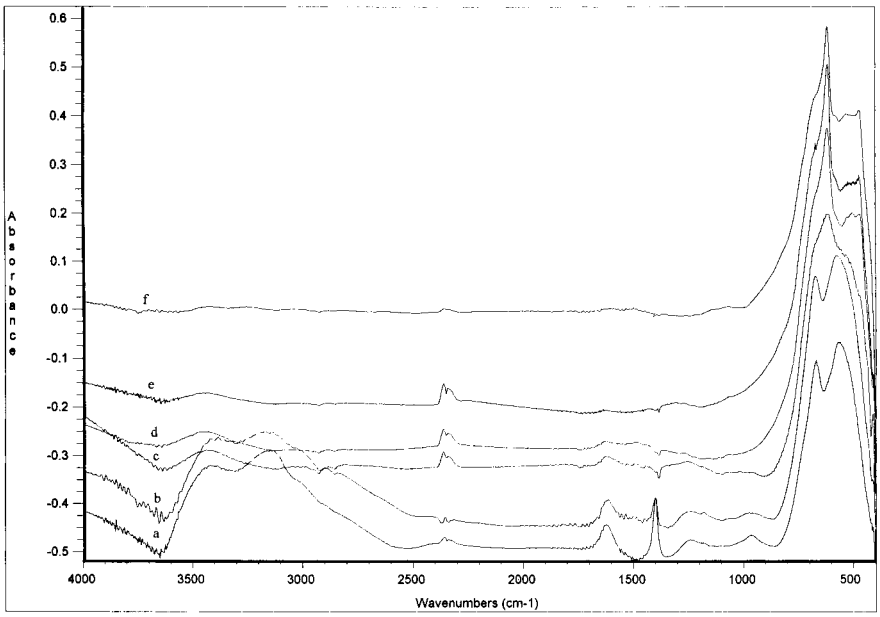

Figure 6. FTIR spectra of SnO_2: (a) as-prepared SnO_2; (b) sintered at 200 °C; (c) 400 °C; (d) 600 °C; (e) 800°; and (f) 1000 °C.

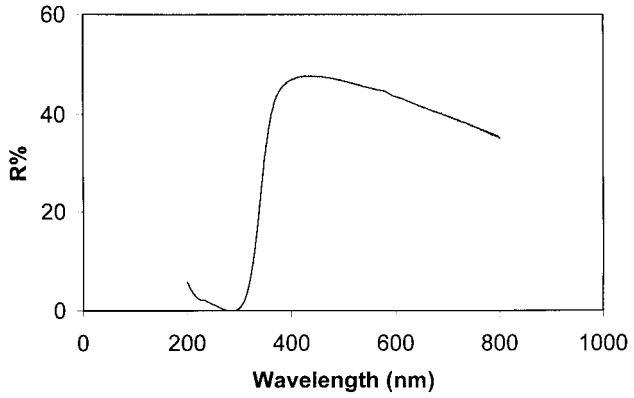

Figure 7. Reflection spectrum of a glass coated with as-prepared SnO_2 nanoparticles.

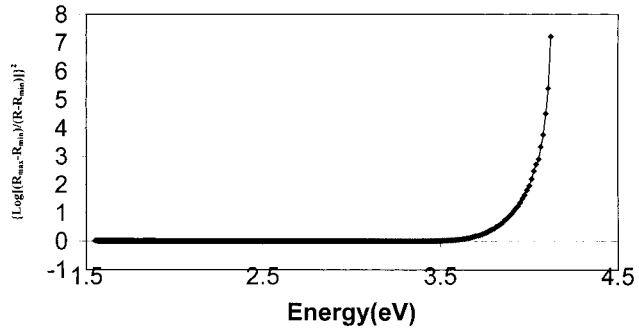

Figure 8. The plot of $\{\log[(R_{max} - R_{min})/(R - R_{min})]\}^2$ vs $h\nu$ (eV) of as-prepared SnO_2.

delithiation cycle of electrodes composed of the as synthesized materials (no heat treatment), and SnO_2 particles heated to 400 and 600 °C, as indicated. It should be noted that the chronopotentiograms of electrodes composed of SnO_2 particles heated to 800 and 1000 °C are very similar to those of the electrodes composed of the materials heated to 600 °C. As shown in Figure 9, the chronopotentiogram related to the as-prepared (least crystalline) SnO_2, reflects a nearly monotonic cathodic process. The curve relating to the lithiation process does not have any plateaus that

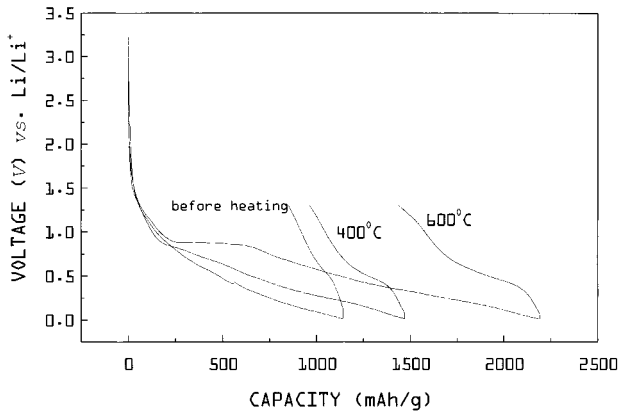

Figure 9. Chronopotentiograms (potential vs capacity curves) recorded during the first lithiation−delithiation cycle (0.2 mA/cm^2) of an electrode composed of unheated, as-prepared SnO_2 nanoparticles and electrodes composed of SnO_2 after heat treatment at 400 °C and 600 °C, as indicated.

usually reflect phase formation or transition. The onset of the cathodic process seems to be a potential below 1.5 V vs Li/Li^+. As found in previous studies,[15,37] the alkyl carbonate solvents are reduced on nonactive metal electrodes at potentials below 1.5 V.[15] This reduction process leads to the precipitation of surface films comprised of $ROCO_2Li$ species, which are the major alkyl carbonate reduction products as the dominant components.[15]

As can be concluded from previous work,[11−14,16] Li_2O is formed below 1 V (Li/Li^+), and at potentials below 0.6 V, Li−Sn alloying processes, which may form a number of Li_xSn components,[11−14,16,38] take place. Hence, the cathodic chronopotentiograms in Figure 9 (first lithiation process) should reflect all these three processes. In contrast to the cathodic process, the chronopotentiogram related to delithiation of the unheated, as-prepared material, has a deflection point around 0.6 V, which probably reflects decomposition of

(37) Aurbach, D.; Levi, M. D.; Levi, E.; Schechter, A. *J. Phys. Chem. B* **1997**, *101*, 2195.

one of the Li−Sn alloys, probably Li_2Sn_5.[12] From these curves it appears that the reversible capacity of this electrode is around 300 mAh/g. This capacity is definitely not lower than that reported in the literature for other types of *practical* Li−Sn electrodes.[38] The irreversible capacity is around 800 mAh/g, probably due to the reduction of solution components that form surface films, and formation of Li_2O according to the following equation:

$$4Li^+ + 4e^- + SnO_2 \rightarrow 2Li_2O + Sn$$

As shown in Figure 9, heat treatment of the SnO_2, which increases its crystallinity (Figure 1), drastically changes the electrochemical behavior of the materials:

1. The reversible capacity in the first lithiation−delithiation cycles increases from around 300 mAh/g to values as high as 800 mAh/g (almost 3-fold), corresponding to 1050 and 2800 mAh/L, respectively.

2. The irreversible capacity also increases (but by a lesser percentage) from around 800 mAh/g for the as-prepared material, to around 1400 mAh/g (∼70%), corresponding to 2800 and 4900 mAh/L, respectively.

3. The lithiation curve has a pronounced and clear plateau around 0.9 V (Li/Li^+), which probably relates to the Li_2O formation. The delithiation curve is characterized by a plateau around 0.5 V.

4. A more rigorous analysis of these potentiograms by their derivatization d*Q*/d*V* indicates distinctive reduction processes (appearing as peaks) at 0.6, 0.3, and 0.2 V (Li/Li^+) and corresponding oxidation processes around 0.4 and 0.65 V (Li/Li^+), which probably relate to different Li−Sn alloying processes.

Hence, it is clear that crystallization of the SnO_2 nanoparticles increases the accessibility of the active mass to the lithium ions and electrons as well, and thus its conversion to Li_2O and Li−Sn alloys by cathodic polarization is more complete in the nanocrystalline form than in the more amorphous state. The plateaus in the chronopotentiograms and the distinctive peaks in the d*Q*/d*V* vs *V* curves reflect processes occurring via phase transition, which is, of course, relevant to crystallinic active mass.

Figure 10 shows chronopotentiograms obtained from the various types of active mass (as-prepared and heat-treated SnO_2) during repeated 20 lithiation−delithiation cycles. Figure 11 compares the charges involved in the lithiation and delithiation processes (discharge and charge, respectively), along 20 cycles for the various types of SnO_2 particles. Finally, Figure 12 compares the first cycle reversible and irreversible capacity to the 20th cycle reversible capacity for the as-prepared SnO_2 and the various heat treated materials (400 °C → 1000 °C). It is clear from Figures 10−12 that crystallization of the SnO_2 nanoparticles considerably increases the reversible capacity of their lithiation. However, this capacity slightly, and gradually, decreases upon cycling. For most of the heat treated samples, a capacity fading of about 50% is recorded during 20 charge−discharge cycles (see comparison in Figure 12). It is very significant that the lowest capacity fading upon cycling (close to zero) was recorded with electrodes composed of the

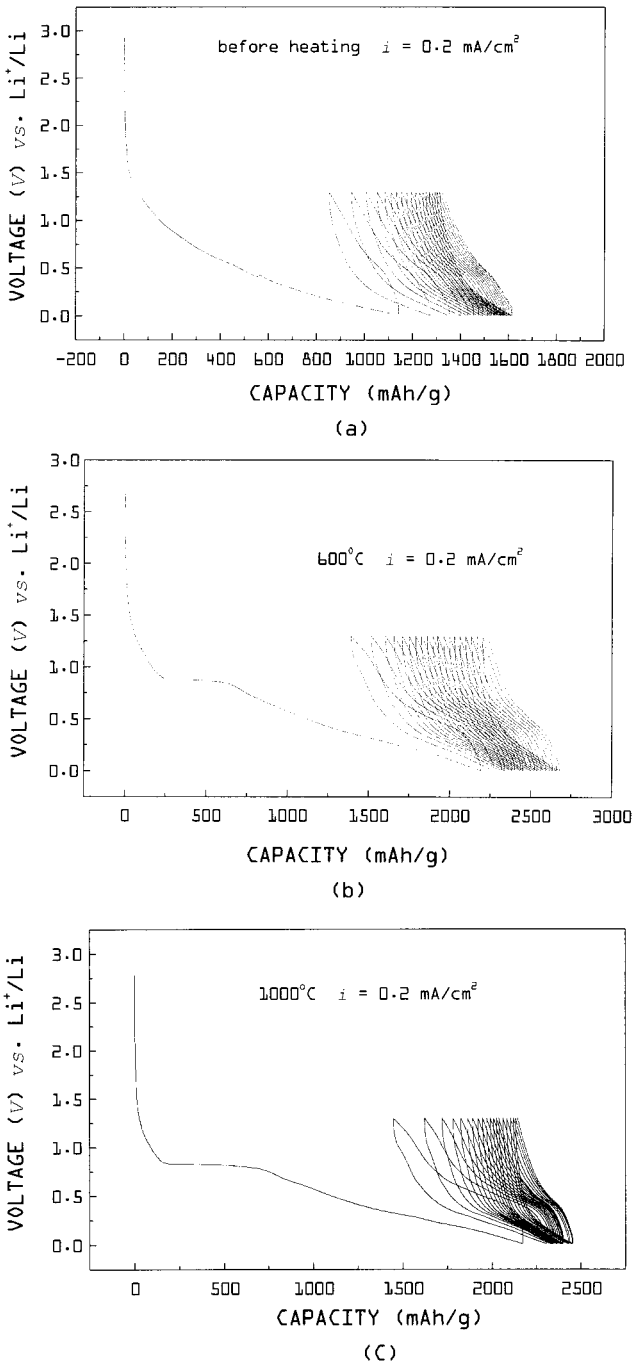

Figure 10. Chronopotentiograms (potential vs capacity curves) of the first 20 discharge and charge galvanostatic cycles of composite electrodes comprised of SnO_2 particles (55%), carbon black (35%), and PVDF binder (15%). $i = 0.2$ mA/cm²: (a) as-prepared sample; (b) heat-treated to 600 °C; and (c) heat-treated to 1000 °C.

more amorphous, as-prepared SnO_2 nanoparticles. Hence, in this paper we address an interesting phenomenon: The capacity of the amorphous SnO_2 nanoparticles in electrochemical lithium insertion is lower compared with the more crystalline materials (produced by heat treatment). However, the capacity fading during prolonged, repeated cycling is also lower for the amorphous SnO_2 particles compared with the more crystalline material. At the moment we do not have an explanation for these results (which are based on solid experimental results). However, we can speculate that lower capacity

(38) Machill, S.; Shodai, T.; Sakurai, Y.; Yamaki, I. J. *J. Power Sources* **1998**, *73*, 216.

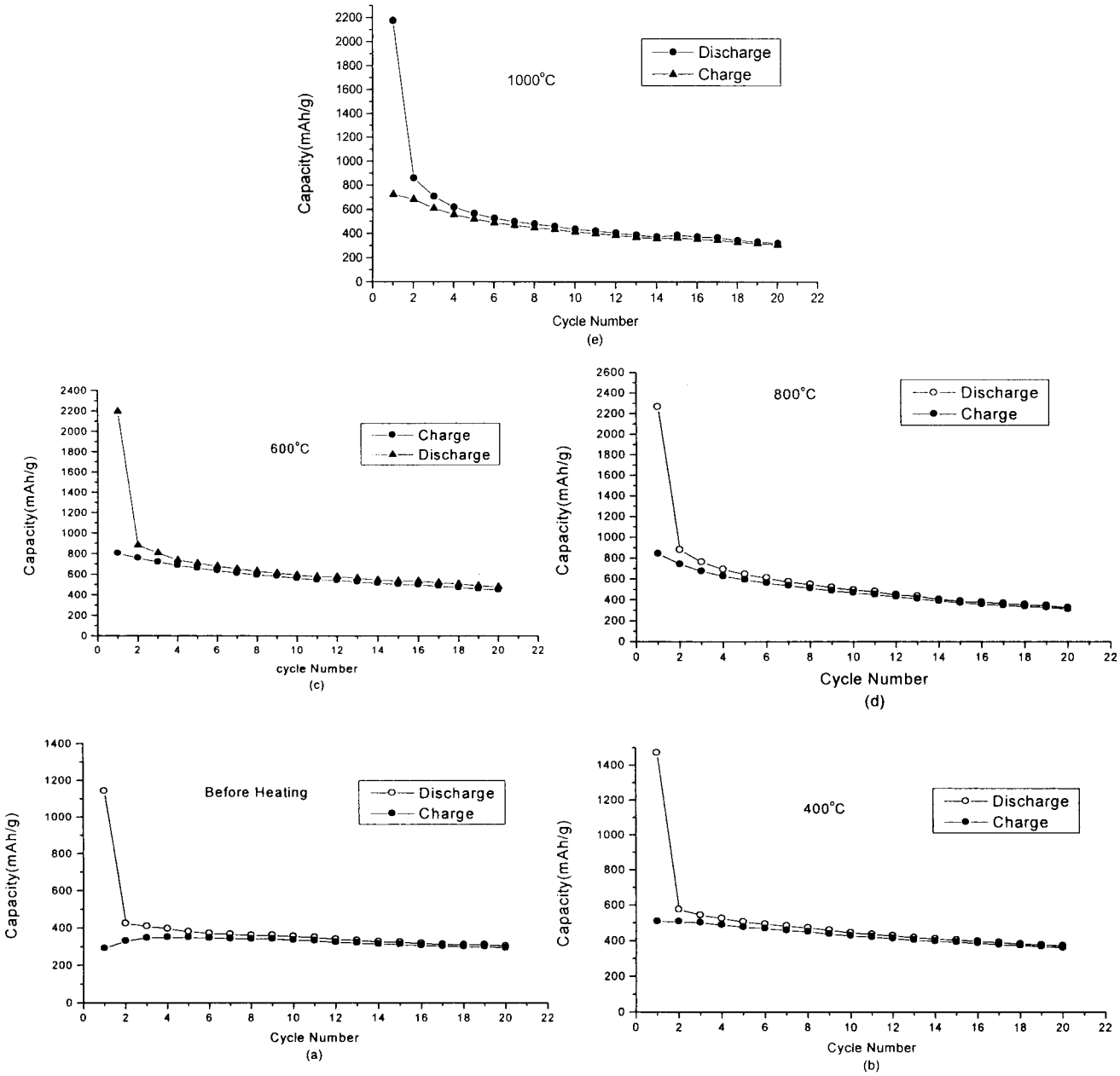

Figure 11. Plots of capacity vs cycle number: (a) as-prepared SnO_2; (b) sintered at 400 °C; (c) 600 °C; (d) 800 °C; (e) 1000°.

fading upon cycling relates to a better interparticle contact in the composite electrodes. However, further studies are required to resolve this issue. Despite the capacity fading of the electrodes composed of the heat-treated SnO_2, upon cycling the preliminary results thus obtained are very promising because it is clear that there is room for further optimization of both the features of the active mass and the electrode structure. The results indicate the strong impact of the heat treatment temperature on the reversible capacity and the capacity fading. It is also expected that optimizing the amount of binder and carbon in the electrodes may have a positive impact on its stability upon cycling. Since the irreversibility also relates to reactions of the active mass with solution components, it is clear that optimization of the solution composition may enhance the electrodes' stability and decrease irreversible phenomena. Hence, this study seems to demonstrate that synthesis of SnO_2 nanoparticles by sonochemical methods followed by optimized heat treatment, may produce anode materials for Li batteries, which may be of practical importance.

4. Conclusion

In this work, a sonochemical method has been used for the preparation of SnO_2 semiconductor nanoparticles. The SnO_2 particles thus prepared were characterized by powder X-ray diffraction (XRD), reflection spectroscopy, FT-IR spectroscopy, transmission electron microscopy (TEM), DSC, and TGA. Preliminary electrochemical tests were performed for studying the behavior of electrodes containing SnO_2 as the active mass, in Li battery solutions. These tests clearly indicated that the SnO_2 particles prepared by sonochemical synthesis have promising capacity, reversibility, and cycle life in repeated lithium insertion and deinsertion processes. Heat treatment of the sonochemically pre-

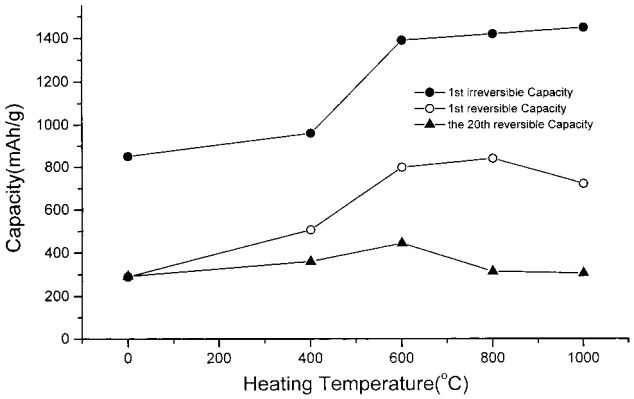

Figure 12. Comparison of capacity as a function of heating temperature and cycle number: (a) reversible capacity in the 20th cycle; (b) first cycle's reversible capacity; and (c) first cycle's irreversible capacity.

pared SnO_2 nanoparticles had a pronounced effect on their electrochemical behavior. The crystallization of the particles due to the heat treatment increased both the electrode's irreversible and reversible capacities measured during the first lithiation−delithiation cycle. However, while the reversible capacity retention upon cycling of electrodes made of as-prepared SnO_2 material was good, the capacity of electrodes made of the heat treated materials degrades upon cycling. We speculate that this can be attributed to problems of electrical integrity of the active mass when its nature is more crystalline. It is assumed that by optimization of heat treatment and solution composition, it is possible to improve the performance of these materials for reversible lithium insertion electrodes. Hence, this work demonstrates that sonochemistry may serve as a useful synthetic tool for producing promising electrode materials for high-energy density batteries.

Acknowledgment. Professor A. Gedanken and Professor D. Aurbach thank the German Ministry of Education and Research through the Deutsche-Israeli Program (DIP) and the Israel National Science Foundation (NSF) for their support, and gratefully acknowledge receipt of a NEDO International Joint Research Grant. They also acknowledge a grant awarded by The Israel SCIENCE FOUNDATION founded by the Israel Academy of Sciences and Humanities. Dr. Zhu thanks the Kort 100 Scholarship Foundation for supporting his postdoctoral fellowship. Dr. Zhu is also grateful for the support of the Chinese Scholarship Council.

CM990683L